Chem Soc Rev

TUTORIAL REVIEW

Double-stranded dimetallic helicates: assembling–disassembling driven by the Cu^{I}/Cu^{II} redox change and the principle of homochiral recognition

Massimo Boiocchi[a] and Luigi Fabbrizzi*[b]

Cite this: DOI: 10.1039/c3cs60428d

Received 26th November 2013

DOI: 10.1039/c3cs60428d

www.rsc.org/csr

In the presence of d^{10} metal ions, prone to tetrahedral coordination, ligands containing several bidentate subunits will give rise to double-stranded helical complexes (helicates). Upon electrochemical oxidation of Cu^{I} to Cu^{II}, the helicate complex tends to disassemble, thus giving rise to two mononuclear Cu^{II} complexes with tetragonal geometry. Upon subsequent Cu^{II}-to-Cu^{I} electrochemical reduction, two Cu^{I} complexes instantaneously re-assemble to give the helicate complex. A helicand containing a chiral subunit (*e.g.* 1,2-substituted cyclohexanediamine) contains a racemic mixture of the *R*,*R* and *S*,*S* enantiomers. The racemic helicand, reacting with Cu^{I}, forms dimetallic helicates, in which the two strands show the same chirality, whether *R*,*R* or *S*,*S*, thus obeying the principle of homochiral recognition.

Key learning points

(1) Sterically constrained linear multidentate ligands may choose to coordinate more metals, arranging themselves in a multiple helical pattern.
(2) d^{10} metal ions (*e.g.* Cu^{I}) tend to arrange quadridentate ligands having a certain degree of rigidity and containing sp^2 nitrogen atoms (pyridine, imine) in a double stranded helicate mode, with a 2 : 2 stoichiometry.
(3) Upon oxidation to Cu^{II}, dicopper(I) helicates disassemble to give mononuclear complexes.
(4) If the helicand is chiral, the metal forms helicates with enantiomeric strands of the same chirality.
(5) In the presence of additional inter-strand interactions (*e.g.* π–π stacking), stable dicopper(II) double-stranded helicates may form.

1 Introduction

Figures consisting of two threadlike objects or living beings intertwined in a double helix mode have attracted and fascinated humans for a long time. In particular, the symbolism of two entwined helical snakes is a recurring motif in the history of humankind.

The first documented example (*ca.* 2100 BC) refers to the 'libation vase of Gudea', a green steatite vase of Sumerian origin, carved to feature the Mesopotamian deity Ningishzida, who was associated with fertility, afterlife and the healing force of nature (see Fig. 1).[1] Ningishzida was portrayed either as a serpent with the head of a man or, more frequently, as a pair snakes entwined around an axial stick. This theme was later borrowed by Greeks when introducing the myth of *caduceus* (see Fig. 2), the wand of Hermes (Mercury for Latins), with two entwined helical snakes, and decorated with a pair of wings.[2]

Fig. 1 The "libation vase of Gudea", dedicated to the Sumerian god Ningishzida (21st century BC): (a) the steatite vase, exhibited in the Louvre, Paris. The photograph displays three different views of the vase: right side, front, left side; (b) drawing illustrating the figures carved in the vase. The double helix depicts the deity.

Hermes, among his many offices, had that of escorting the souls of newly deceased people in the afterlife (*Hermes psychopompos*, 'conductor of souls'), showing in this affinity with the Sumerian god Ningishzida. Hermes/Mercury was also a patron

[a] *Centro Grandi Strumenti, Università di Pavia, via Bassi 21, 27100 Pavia, Italy*
[b] *Dipartimento di Chimica, Università di Pavia, via Taramelli 12, 27100 Pavia, Italy. E-mail: luigi.fabbrizzi@unipv.it*

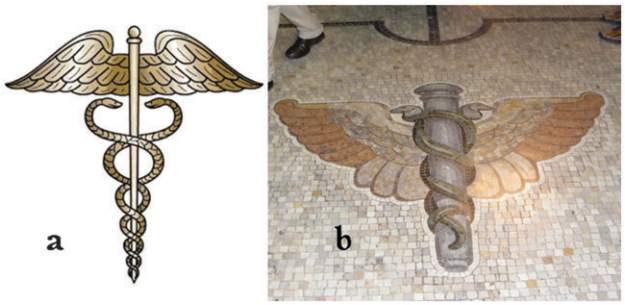

Fig. 2 (a) The *caduceus* (the staff of the herald), typical attribute of Hermes-Mercury; (b) a mosaic featuring the caduceus on the floor at the Central Railroad Station in Milan.

of commerce and trade, which explains the presence of mosaics featuring the caduceus on the floor of the Central Railroad Station in Milan, the Italian capital of trade and commerce (see Fig. 2b).

Quite unexpectedly, the theme of intertwined snakes was also adopted by the Roman Catholic Church. Fig. 3a shows a low relief from the main portal of the romanesque Basilica of Saint Michael in Pavia, featuring two helically arranged snakes.[3] In Catholic teachings, Archangel Michael is the angel of death, carrying the souls of all the deceased to heaven, a function, that of a psychopomp, which establishes a significant link with Ningishzida and Hermes/Mercury. In pagan times, people of Southern Lombardy were especially devoted to Mercury and to the cult of the dead. The Basilica was built to maintain, in a Catholic version, this traditional cult and was entitled to Saint Michael to avert inhabitants from veneration of Mercury, whose typical attributes (including intertwined snakes) were transferred to the Archangel.

The double helix motif had a sensational *entrée* in chemistry in 1953, with Crick and Watson's disclosure of the structure of DNA.[4] Since then, the double helix has rightfully become a recurring and fascinating theme of chemical design.[5]

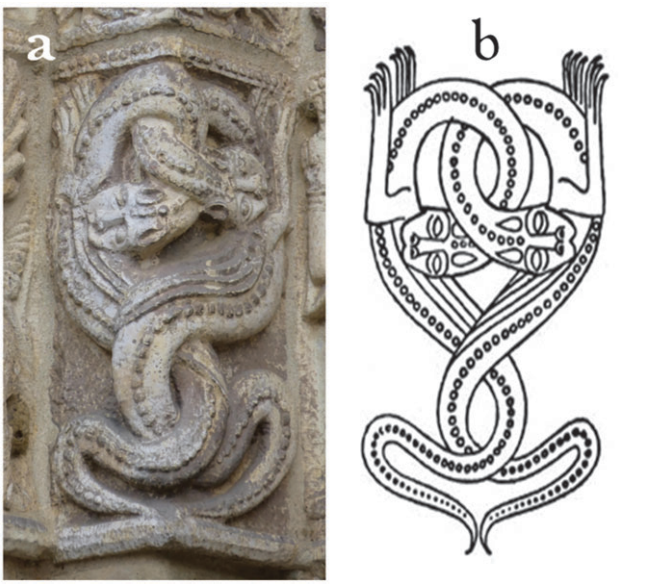

Fig. 3 (a) A low relief featuring two intertwined snakes in the main portal of the romanesque Basilica of Saint Michael in Pavia (completed in 1125 AD); (b) a drawing illustrating the subject featured in the low relief.

In 1987, Lehn reported one of the first examples of ''inorganic double helices'', *i.e.* a class of Cu^{I} polynuclear metal complexes in which two linear polypyridine ligands are wrapped around two or three metals, forming a double helix.[6] In the line of the nomenclature introduced for cryptands and cryptates,[7] corresponding ligands were called *helicands* and their complexes *helicates*. Fig. 4 shows the crystal and molecular structure of a trisilver(I) double stranded helicate.[6]

Both DNA and metal helicates are held together by non-covalent interactions (hydrogen bonding and coordinative interactions, respectively), a feature which permits the achievement, through self-assembling, to give elaborate structures, *via*

Massimo Boiocchi

Massimo Boiocchi was born in Pavia in 1971. In 2000 he received his PhD degree in 'Mineralogy, Petrology and Crystallography' from the University of Pavia, under the supervision of Professor Luciano Ungaretti. Since 2002, he has been a research technician in the Laboratory of Crystallography of Centro Grandi Strumenti of the University of Pavia. He is currently interested in the structural aspects of metal containing supramolecular systems, with particular interest in chiral compounds.

Luigi Fabbrizzi

Luigi Fabbrizzi was born in 1946 in Florence, where he received all his education and obtained his degree in Chemistry in 1969. He was a post-doctoral fellow and a lecturer of inorganic chemistry at the University of Florence until 1980, when he was appointed as a Professor of Chemistry at the University of Pavia. His research interests cover several aspects of supramolecular chemistry, including metal directed self-assembling, anion recognition and sensing, and molecular devices. He is Honorary Professor of the East China University of Science and Technology in Shanghai. He was the recipient of the 2010 Izatt–Christensen Award in Macrocyclic Chemistry.

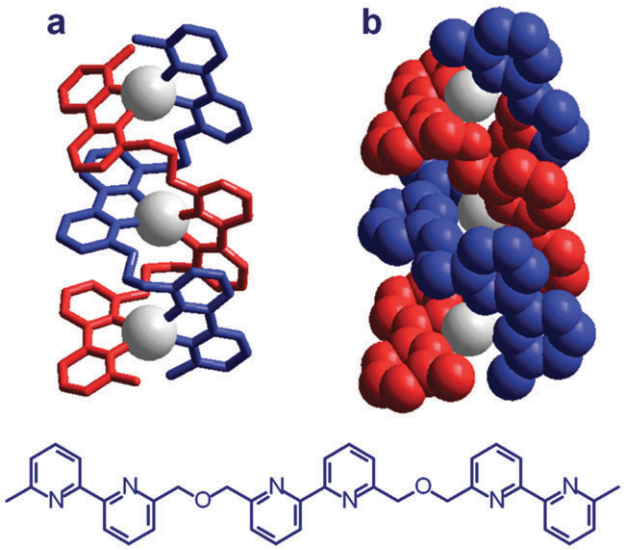

Fig. 4 Crystal and molecular structure of the $[Ag^{I}_3(\mathbf{L})_2](CF_3SO_3)_3$ complex salt.[6] Formula of the ligand **L** is reported in the figure: (a) tube representation of the trinuclear double stranded helicate complex $[Ag^{I}_3(\mathbf{L})_2]^{3+}$; (b) space filling rendering. Counterions and hydrogen atoms have been omitted for clarity.

a repetitive trial-and-error mechanism. The double stranded structure of helicate complexes results from the balance between (i) the coordinative geometrical preferences of the metal ion and (ii) the steric constraints intrinsically present in the linear ligand, which may disfavour the formation of a mononuclear complex. Tetrahedral and octahedral complexes possess a helical twist and are good candidates for the formation of helicates.[8] In fact, first double-stranded helicates were obtained with post-transition d^{10} metal ions (Cu^{I}, Ag^{I}), well inclined to a tetrahedral coordination geometry.[9] Genuine transition metals like Co^{II} and Ni^{II} have a strong preference for octahedral coordination and form either double-stranded helicates with ligands bearing terdentate subunits or triple stranded helicates, if the ligand possesses bidentate coordinating subunits.[10] Copper is a special case: in the presence of a bis-bidentate ligand **L**∩**L**, the Cu^{I} ion will form a stable dinuclear double-stranded helicate $[Cu^{I}_2(\mathbf{L}\cap\mathbf{L})_2]^{2+}$. On the other hand, the Cu^{II} ion shows a definite preference for tetragonal coordination, a geometrical arrangement which does not possess a pronounced helical twist and, in the absence of particular steric constraints, it will tend to form with **L**∩**L** a mononuclear complex, $[Cu^{II}(\mathbf{L}\cap\mathbf{L})]^{2+}$, of square geometry (or of a related geometry: square pyramid, elongated octahedron).

These contrasting features may allow an operator to promote and control the process of assembling–disassembling a double helix complex through the Cu^{II}/Cu^{I} redox change, in a consecutive way, at will, according to the equilibrium illustrated in Fig. 5. This aspect will be discussed in detail in the present *tutorial* Review.

2 Control of the Cu^{II}/Cu^{I} redox couple through metal–ligand interactions

A number of transition metals display two main oxidation states of comparable stability, *e.g.* Co^{II} and Co^{III}, Fe^{II} and Fe^{III},

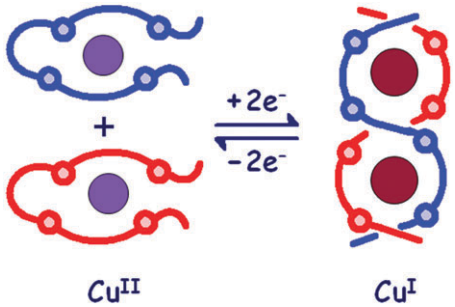

Fig. 5 The process of assembling–disassembling a dimetallic double-stranded helicate complex through the Cu^{II}/Cu^{I} redox change.

Ru^{II} and Ru^{III} *et cetera*. A change of the oxidation state typically induces a pronounced modification of electronic properties, absorption spectra and magnetism. The relative stability of the two oxidation states, which is expressed by the potential of the corresponding redox couple, $E^{\circ}(M^{(n+1)+}/M^{n+})$, can by modulated by the nature of the coordinated ligands, including solvent. Probably, the most drastic change of the chemical properties is observed with the Cu^{II}/Cu^{I} couple. In fact, Cu^{II}, d^9, is a genuine transition metal ion, which profits from ligand field stabilisation energy and, depending upon the structural features of the multidentate ligand, can adopt a variety of geometries, from square planar to five-coordinate (either square pyramidal or trigonal bipyramidal) to octahedral. On the other hand, Cu^{I}, d^{10}, is a post-transition, 'spherical' metal ion, the geometry of its complexes is only sterically determined and it tends to adopt a tetrahedral coordination geometry. There exist also substantial differences in bonding properties: the *borderline* Cu^{II} ion establishes with the donor atoms only σ interactions, whereas Cu^{I} is capable of back donating electrons to π-acceptor ligands (*e.g.* polypyridines), which makes it belong to the class of *soft* metal ions.[11] An illustrative example is provided by the complexes of 2,2′-bipyridine (bpy). Cu^{I} gives with bpy a 1 : 2 complex with an intense brick-red colour (due to an MLCT transition). Fig. 6a displays the X-ray determined structure of the $[Cu^{I}(bpy)_2]^{+}$ complex (counterion $CF_3SO_3^{-}$).[12]

The Cu^{I} complex shows a slightly distorted tetrahedral geometry: in particular, the angle between the planes containing the five-membered chelate rings, Φ, is 84° ($\Phi = 90°$ for a regular tetrahedron and =0° for a square planar coordination geometry). On the other hand, the crystalline complex salt $[Cu^{II}(bpy)_2](BF_4)_2$ (Fig. 6b) shows a flattened arrangement of the two bpy molecules, to give a rather distorted square planar coordination geometry.[13] Deviation from planarity may be ascribed (i) to steric repulsions between the two ligands and (ii) to the Jahn–Teller effect, which operates for a d^9 complex, in a square coordinative arrangement. It has to be noted that an anion or a solvent molecule, if present in the crystal, may be involved in the coordination. The complex is five-coordinate, according to a trigonal bipyramidal geometry, with the anion or the solvent molecule occupying one of the three equatorial positions. This is the case, for instance, of the complex salt $[Cu^{II}(bpy)_2(H_2O)](BF_4)_2$, whose structure is shown in Fig. 6c.[14] As far as the solution behaviour is concerned, it is suggested that the copper(II) complex assumes the distorted square planar geometry in poorly coordinating solvents

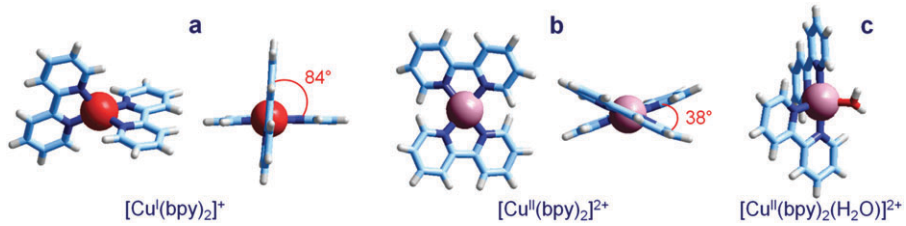

Fig. 6 Crystal and molecular structures of copper complex salts with 2,2′-bipyridine (bpy): (a) $[Cu^{I}(bpy)_2]CF_3SO_3$, nearly regular tetrahedral geometry;[12] (b) $Cu^{II}(bpy)_2](BF_4)_2$, very flattened tetrahedral geometry;[13] (c) $[Cu^{II}(bpy)_2(H_2O)](BF_4)_2$, trigonal bipyramidal geometry, with the coordinated water molecule occupying an equatorial position.[14] Anions and 2,2′-bipyridine hydrogen atoms have been omitted for clarity.

(*e.g.* CH_2Cl_2, $CHCl_3$), in the presence of poorly coordinating anions, and the trigonal bipyramidal arrangement in coordinating solvents (water, MeCN).

These drastic changes in coordination geometry and binding properties have been used to promote, through the Cu^{II}/Cu^{I} change, a variety of processes, including molecular motions. The first and probably most spectacular example refers to the half turn of one ring of a 2-catenane containing phenanthroline and terpyridine subunit, induced by the Cu^{I}/Cu^{II} couple.[15] The same redox process has been used to promote copper translocation between the two compartments of a ditopic ligand.[16] Recently, the redox driven interconversion between a dinuclear Cu^{I} double helicate and a tetranuclear Cu^{II} grid has been reported.[17]

3 Assembling–disassembling dicopper(I) double-stranded helicates with quaterpyridine ligands

An intriguing application of the Cu^{II}/Cu^{I} change involves the redox driven processes of assembling–disassembling double-stranded dimetallic helicates.

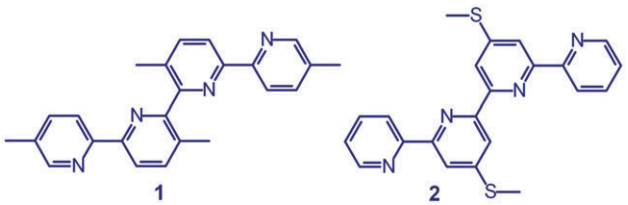

There exist quadridentate ligands, like **1**, which, in spite of quite severe steric constraints, are able to coordinate a Cu^{II} ion according to a slightly distorted tetragonal arrangement. In particular, as shown by X-ray diffraction studies on the salt $[Cu^{II}(\mathbf{1})(H_2O)](ClO_4)_2$,[19] the $[Cu^{II}(\mathbf{1})(H_2O)]^{2+}$ complex shows a square pyramidal geometry, in which the four nitrogen atoms of quaterpyridine **1** occupy the corners of the basal square, while the apical position is held by a water molecule (see Fig. 7).

The Cu^{II} ion is displaced from the plane of the four nitrogens, towards the water molecule, by 0.18 Å. Notice that the corresponding complex $[Cu^{II}(bpy)_2(H_2O)]^{2+}$,[14] shown in Fig. 6, presents a trigonal bipyramidal coordination geometry. The intrinsically less stable square pyramidal arrangement of the $[Cu^{II}(\mathbf{1})(H_2O)]^{2+}$ complex is probably induced by steric constraints associated with the quaterpyridine framework.

On the other hand, quaterpyridine **1**, when coordinating the Cu^{I} ion, finds it difficult to place its four nitrogen atoms at the vertices of a tetrahedron in a 1 : 1 complex. Thus, it prefers to give a 2 : 2 complex, in which each Cu^{I} ion is coordinated by two nitrogen atoms of one quaterpyridine strand and by two nitrogen atoms of the other quaterpyridine strand (see the X-ray determined structure of the $[Cu^{I}_2(\mathbf{1})_2](ClO_4)_2{\cdot}H_2O$ complex salt in Fig. 7b and c).[19] In the dinuclear complex, each metal experiences a slightly distorted tetrahedral coordination (Φ = 80.0°). The two molecules of **1** are arranged to give a double helix. $[Cu^{I}_2(\mathbf{1})_2]^{2+}$ is the very first example of double stranded helicate complexes.

Very interestingly, in an MeCN solution, the two-electron oxidation of two mononuclear $[Cu^{II}(\mathbf{1})]^{2+}$ complexes induces the

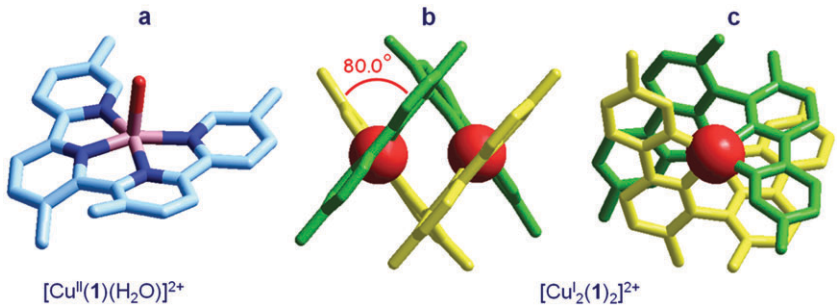

Fig. 7 Crystal and molecular structures of the complex salts: (a) $[Cu^{II}(\mathbf{1})(H_2O)](ClO_4)_2$;[18] (b) $[Cu^{I}_2(\mathbf{1})_2](ClO_4)_2{\cdot}H_2O$;[19] (c) the same as (b), view along the axis containing the two Cu^{I} ions. The double helix in (b) shows *M*-handedness (left-handed). In the unit cell of the centrosymmetric crystal, both *M* and *P* helices are present. Anions, solvate water molecules and quaterpyridine hydrogen atoms have been omitted for clarity.

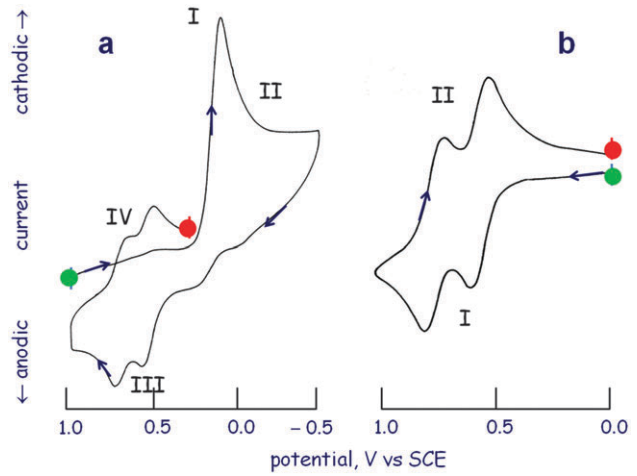

Fig. 8 (a) CV profile taken on an MeCN solution 0.1 M in tetraethylammonium perchlorate and 5×10^{-4} M in $[Cu^{I}_2(\mathbf{1})_2]^{2+}$ (diagram adapted from ref. 18). Since the working platinum electrode has been set at 1.0 V *vs.* SCE, the complex in the layer around the electrode has been converted to the mononuclear $[Cu^{II}(\mathbf{1})]^{2+}$ complex, on which the CV experiment has been carried out. Filled green circle, start; I, reduction of $[Cu^{II}(\mathbf{1})]^{2+}$ to $[Cu^{I}(\mathbf{1})]^{+}$; II, self-assembling of two $[Cu^{I}(\mathbf{1})]^{+}$ to give the $[Cu^{I}_2(\mathbf{1})_2]^{2+}$ helicate complex; III, stepwise one-electron oxidation of $[Cu^{I}_2(\mathbf{1})_2]^{2+}$ to $[Cu^{II}Cu^{I}(\mathbf{1})_2]^{3+}$ and to $[Cu^{II}_2(\mathbf{1})_2]^{4+}$; IV, stepwise one-electron reduction of $[Cu^{II}_2(\mathbf{1})_2]^{4+}$ to $[Cu^{II}Cu^{I}(\mathbf{1})_2]^{3+}$ and to $[Cu^{I}_2(\mathbf{1})_2]^{2+}$; filled red circle, stop. (b) CV profile taken on an MeCN solution 0.1 M in tetraethylammonium perchlorate and 7.8×10^{-4} M in the $[Cu^{II}(\mathbf{1})]^{2+}$ complex. Since the working platinum electrode has been set at 0.0 V *vs.* SCE, the complex in the layer around the electrode has been converted to the dinuclear $[Cu^{I}_2(\mathbf{1})_2]^{2+}$ helicate complex, on which the CV experiment has been carried out. Two one-electron oxidation processes of the integer dimetallic complex are observed, at a scan rate of 100 mV s^{-1} (I) followed by two stepwise one-electron reduction processes (II). Filled green circle, start; filled red circle, stop.

formation of the double stranded helicate $[Cu^{I}_2(\mathbf{1})_2]^{2+}$.[18] The occurrence of the assembling process is nicely demonstrated by the cyclic voltammetry (CV) profile, shown in Fig. 8a.

The experiment deserves a detailed description. The working platinum electrode was dipped in an MeCN solution, made 0.1 M in tetraethylammonium perchlorate and 5×10^{-4} M $[Cu^{I}_2(\mathbf{1})_2]^{2+}$. The potential of the working electrode was set at 1.0 V *vs.* the reference electrode, SCE. At this potential, the dicopper(II) complex in the layer around the working electrode was oxidised to $[Cu^{II}(\mathbf{1})]^{2+}$. In the CV experiment, the potential was scanned from 1.0 V (green filled circle, in Fig. 8a, start) to −0.5 V, then reversed to 1.0 V and scanned again until 0.25 V (red filled circle, stop), at a rate of 100 mV s^{-1}. Upon the first reduction scan, a cathodic peak appeared, with a maximum at ~0.1 V (I), which corresponds to the reduction of the mononuclear complex $[Cu^{II}(\mathbf{1})]^{2+}$ to the mononuclear $[Cu^{I}(\mathbf{1})]^{+}$. Then, the two metastable $[Cu^{I}(\mathbf{1})]^{+}$ complexes assembled to give the dimeric helicate complex $[Cu^{I}_2(\mathbf{1})_2]^{2+}$ (a process occurring in the portion II of the reduction scan, see Fig. 8). Then, upon the reverse scan, two waves appeared, separated by 200 mV (III), corresponding (i) to the one-electron oxidation of $[Cu^{I}_2(\mathbf{1})_2]^{2+}$ to the $[Cu^{II}Cu^{I}(\mathbf{1})_2]^{3+}$ mixed valence complex, and (ii) to the oxidation of $[Cu^{II}Cu^{I}(\mathbf{1})_2]^{3+}$ to $[Cu^{II}_2(\mathbf{1})_2]^{4+}$. Upon the subsequent reverse scan, the two corresponding reduction waves developed (IV), demonstrating the reversibility of the two

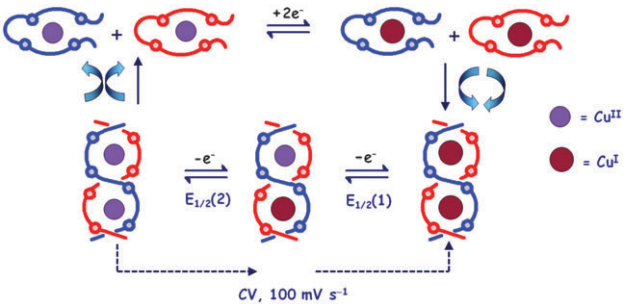

Fig. 9 Scheme of the electrochemical behaviour of copper(II) and copper(I) complexes of helicand **1**, as illustrated by CV profiles in Fig. 8.

stepwise one-electron reduction processes and the integrity of the two dinuclear complexes $[Cu^{II}Cu^{I}(\mathbf{1})_2]^{3+}$ and $[Cu^{II}_2(\mathbf{1})_2]^{4+}$ in the time scale of the CV experiment. The reversibility of the two stepwise one-electron redox processes is clearly illustrated in Fig. 8b. In this case, an MeCN solution of the $[Cu^{II}(\mathbf{1})]^{2+}$ complex was investigated and the potential of the working electrode was set at 0.0 V *vs.* SCE. At this potential, the mononuclear Cu^{II} complex was reduced to Cu^{I} and the dimetallic helicate complex $[Cu^{I}_2(\mathbf{1})_2]^{2+}$ formed. Upon the cyclic scan between 0.0 and 1.0 V the two reversible one-electron waves were observed, with $E_{1/2}$ values: 0.73 V *vs.* SCE ($Cu^{II} \sim Cu^{II} \leftrightarrows Cu^{II} \sim Cu^{I}$) and 0.53 V *vs.* SCE ($Cu^{II} \sim Cu^{I} \leftrightarrows Cu^{I} \sim Cu^{I}$). Since reversibility was observed down to the potential scan rate of 10 mV s^{-1}, over a 1000 mV interval, the lifetime of the two complexes can be estimated to be no lower than 100 s. The voltammetric behaviour illustrated in Fig. 8a and b is pictorially represented in Fig. 9.

Notice that the $[Cu^{II}_2(\mathbf{1})_2]^{4+}$ complex (left lower corner of the scheme) undergoes a double fate: if not electrochemically perturbed, it slowly decomposes to give two equivalents of the mononuclear complex $[Cu^{II}(\mathbf{1})]^{2+}$; if involved in a CV experiment, it undergoes two reversible one-electron reduction process, to the mixed valence and to the dicopper(I) helicate complexes (dashed line in the bottom of Fig. 9).

The electrochemically controlled assembling–disassembling of a dicopper(I) double stranded helicate was also investigated for quaterpyridine **2**.[20] The ligand contains two thioetereal substituents, but there is not evidence for the coordination of the sulphur atoms to Cu^{I} and Cu^{II} metal centres. Fig. 10 shows the crystal and molecular structure of the complex salt $[Cu^{II}_2(\mathbf{2})_2](PF_6)_2 \cdot MeCN$.[20]

In spite of the rather strict similarity of helicand **1** and **2**, the $[Cu^{I}_2(\mathbf{2})_2]^{2+}$ complex shows distinct differences from the $[Cu^{I}_2(\mathbf{1})_2]^{2+}$ analogue. In particular, the coordination tetrahedron of each Cu^{I} centre is rather flattened, with an angle Φ = 68°. As a consequence the $Cu^{I} \cdots Cu^{I}$ distance is especially short (3.32 Å), to be compared to the value of 3.90 Å observed in the $[Cu^{I}_2(\mathbf{1})_2]^{2+}$ helicate. As far as the Cu^{II} complex is concerned, a microcrystalline compound of formula $[Cu^{II}(\mathbf{2})(CH_3OH)](PF_6)_2$ was isolated, for which a structure similar to that observed for the $[Cu^{II}(\mathbf{1})(H_2O)]^{2+}$ complex was suggested, the water molecule of the latter complex being replaced by a methanol molecule.

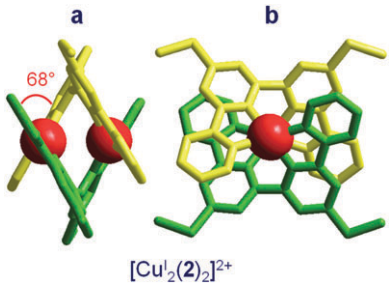

Fig. 10 Crystal and molecular structure of the complex salt [Cu$^{II}_2$(**2**)$_2$](PF$_6$)$_2$·MeCN.[20] Anions, solvate MeCN and quaterpyridine hydrogen atoms have been omitted for clarity. (a) Lateral view and (b) view along the axis containing the two Cu^{I} centres of the [Cu^{II}(**2**)]$^{2+}$ complex. The double helix shows *P*-handedness (right-handed). In the unit cell of the centrosymmetric crystal both *M* and *P* helices are present.

Distinctive differences were observed also in the electrochemical behaviour. Fig. 11a shows the CV profile obtained at a platinum working electrode for a DMSO solution of [Cu^{II}(**2**)(CH$_3$OH)](PF$_6$)$_2$, made 0.1 M in tetrabutylammonium perchlorate.

Upon decreasing the potential a one-electron irreversible reduction is observed (I in Fig. 11a), with E_p = −0.06 V corresponding to the reduction of Cu^{II} to Cu^{I}. Following the reduction (portion II of the CV profile), the complex rapidly dimerizes to form the helicate complex [Cu$^{II}_2$(**2**)$_2$]$^{2+}$. Then, upon scan reversal, the dicopper(I) complex undergoes a two-electron process (III, E_p = 0.38 V), in which both Cu^{I} centres are oxidized to Cu^{II}, to give the dicopper(II) helicate complex. Such a dinuclear species is unstable and rapidly disassembles to give two equivalents of the monomeric complex Cu^{II}(**2**)]$^{2+}$ (IV). The discussed CV behaviour is pictorially illustrated in the square scheme shown in Fig. 12.

It has to be noted that the [Cu$^{II}_2$(**2**)$_2$]$^{4+}$ complex is not stable in solution in the time scale of the CV experiment. As it fully decomposes in a 400 mV interval, at a scan rate of 100 mV, it

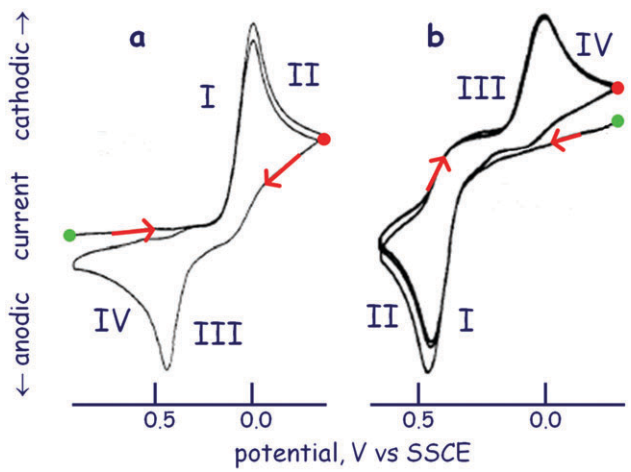

Fig. 11 CV profiles obtained at a platinum working electrode for DMSO solutions, made 0.1 M in tetrabutylammonium perchlorate, of (a) [Cu^{II}(**2**)(CH$_3$OH)](PF$_6$)$_2$, (b) [Cu$^{II}_2$(**2**)$_2$](PF$_6$)$_2$ (diagrams adapted from ref. 20). Potential scan rate: 100 mV s^{-1}. Green filled circle, start of the potential scan; red filled circle, stop.

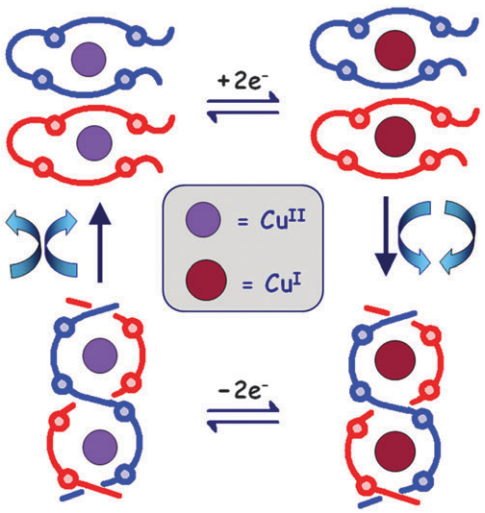

Fig. 12 Square scheme illustrating the processes observed in the CV profile shown in Fig. 11a.

should have a life time lower than 4 s, to be compared to the [Cu$^{II}_2$(**2**)$_2$]$^{4+}$ analogue, for which a lifetime higher than 100 s had been estimated. The much lower stability can be tentatively explained considering that the metal–metal distance is much smaller in the [Cu$^{II}_2$(**2**)$_2$]$^{4+}$ complex than in the [Cu$^{II}_2$(**1**)$_2$]$^{4+}$ (3.32 Å and 3.90 Å, respectively). If such a large difference of metal–metal distances is maintained in the corresponding Cu^{II} helicate complexes, an especially high electrostatic repulsion should operate in [Cu$^{II}_2$(**2**)$_2$]$^{4+}$, causing rapid disassembling to the two monometallic complexes.

The instability of the [Cu$^{II}_2$(**2**)$_2$]$^{4+}$ complex was confirmed by CV studies on a DMSO solution of the [Cu$^{II}_2$(**2**)$_2$](PF$_6$)$_2$ complex salt, illustrated in Fig. 11b. In this case, the scan of the potential was started at −0.35 V and the potential was increased up to 0.60 V. An irreversible peak was observed at 0.38 V, corresponding to the two-electron oxidation of [Cu$^{I}_2$(**2**)$_2$]$^{2+}$. Upon the reverse scan, the corresponding reduction peak was not observed, suggesting that the disassembling of the electrogenerated [Cu$^{II}_2$(**2**)$_2$]$^{4+}$ complex had rapidly occurred. Instead, an irreversible reduction peak was observed at −0.08 V, to be ascribed to the one-electron reduction of the mononuclear complex [Cu^{II}(**2**)]$^{2+}$ to the metastable species [Cu^{I}(**2**)]$^{+}$, which immediately dimerised to form the helicate again. Also in the present case, the CV behaviour can be pictorially illustrated by the square scheme shown in Fig. 12. The starting point is now the dicopper(I) complex in the right lower corner of the square.

4 Dinucleating Schiff base helicands derived from *trans*-1,2-cyclohexanediamine

A further interesting class of dinucleating helicands has been obtained through the Schiff base condensation of *trans*-1,2-cyclohexanediamine with 2-pyridine-carbaldehyde and its derivatives. For instance, the helicand **3** (see Fig. 13) has been

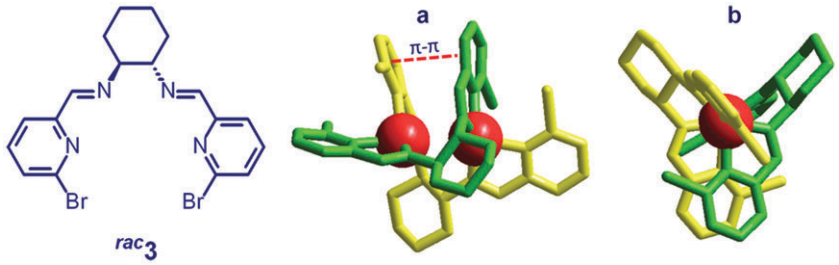

Fig. 13 Crystal and molecular structure of the complex salt $[Cu^{I}_2(\mathbf{3})_2](CF_3SO_3)_2{\cdot}CH_3CN{\cdot}(C_2H_5)_2O$.[21] The unit cell contains the two enantiomeric complexes *M*,*M*-$[Cu^{I}_2(^{RR}\mathbf{3})_2]^{2+}$ and *P*,*P*-$[Cu^{I}_2(^{SS}\mathbf{3})_2]^{2+}$. The structure of the left-handed form (*M*-handedness) is shown in the figure. Hydrogen atoms, anions, solvate molecules and ligand hydrogen atoms have been omitted for clarity; (a) lateral view; (b) view along the axis containing the two Cu^{I} centres.

obtained from the reaction of the racemic form of the diamine with 6-bromo-2-pyridine-carboxyaldehyde.[21]

Ligand **3** contains two bidentate subunits, constituted by two conjugated sp^2 nitrogen atoms (pyridine and imine), suitable for coordination to a π-donor d^{10} cation (*e.g.* Cu^{I}). Metal preference for a tetrahedral coordination and steric constraints present in the ligating system are expected to favour the formation of a dinuclear complex. As ligand **3** is constituted by two enantiomers, $^{R,R}\mathbf{3}$ and $^{S,S}\mathbf{3}$, a further element of complexity is introduced: the matching of the chiral properties of the one strand with the other, when the helicate dicopper(I) complex forms. In particular, it was observed that the reaction of equimolar amounts of $^{rac}\mathbf{3}$ with $[Cu^{I}(MeCN)_4]CF_3SO_3$ in 1 : 1 CH_2Cl_2/MeCN gave rise to a racemic mixture of homochiral dinuclear species *M*,*M*-$[Cu^{I}_2(^{RR}\mathbf{3})_2]^{2+}$ (*i.e.* two intertwined helices, both with *M* handedness) and *P*,*P*-$[Cu^{I}_2(^{SS}\mathbf{3})_2]^{2+}$ (*i.e.* two intertwined helices, both with *P* handedness) in the unit cell. This indicates that, in the formation of the helicate complex, strands of the same chirality seek each other, thus obeying the *principle of homochiral recognition*.[21] The self recognition process is described by equilibrium (1):

$$4Cu^{I} + 2\,^{RR}\mathbf{3} + 2\,^{SS}\mathbf{3} \leftrightarrows M,M\text{-}[Cu^{I}_2(^{RR}\mathbf{3})_2]^{2+} + P,P\text{-}[Cu^{I}_2(^{SS}\mathbf{3})_2]^{2+} \quad (1)$$

The intrinsic substitutional lability of the spherical Cu^{I} ion ensures the fast attainment of the stable homochiral helicate complexes.

Fig. 13 shows two different views of the *M*,*M*-$[Cu^{I}_2(^{RR}\mathbf{3})_2]^{2+}$ enantiomer. Each metal centre displays a rather distorted tetrahedral coordination geometry, which can be better described as a trigonal monopyramid, in which a pyridine nitrogen atom occupies the axial position. The $Cu^{I}\cdots Cu^{I}$ distance is 3.2 Å. It should be noticed that two pyridine rings of two different ligands face each other in a nearly parallel fashion (the angle of the planes containing the pyridine subunits is 29.4°) and the distance between the centroids of the two rings is 3.95 Å, which may account for the occurrence of a π–π interaction. Homochiral recognition has been ascribed to the fact that two rigid units of the same chirality combine to give a compact structure, whereas two heterochiral units give a structure which is less compact.[21] Authors considered that rigidity and steric constraints would prevent tetragonal coordination and did not investigate the possible formation of a mononuclear complex of Cu^{II} with **3**.[21]

On the same route, our group considered the Schiff base **4**, obtained through reaction of racemic 1,2-*trans*-cyclohexanediamine with 2-quinoline-carbaldehyde.[22] Upon reaction of **4** with anhydrous $Cu^{II}(CF_3SO_3)_2$ in MeCN, a deep green solution was obtained, from which, upon slow evaporation, dark green crystals of the mononuclear complex salt $Cu^{II}(\mathbf{4})(CF_3SO_3)_2$ were obtained. Single crystal X-ray diffraction studies showed that crystal contains the two enantiomers *P*-$Cu^{II}(^{SS}\mathbf{4})(CF_3SO_3)_2$ and *M*-$Cu^{II}(^{RR}\mathbf{4})(CF_3SO_3)_2$.

Fig. 14 shows the structure of the *M*-$Cu^{II}(^{RR}\mathbf{4})(CF_3SO_3)_2$ enantiomer.[22] The Cu^{II} cation is coordinated by the four nitrogen atoms of a single quadridentate ligand and lies only 0.03 Å above the N_4 mean-plane, but the four nitrogen atoms are displaced with respect to the plane with distances ranging

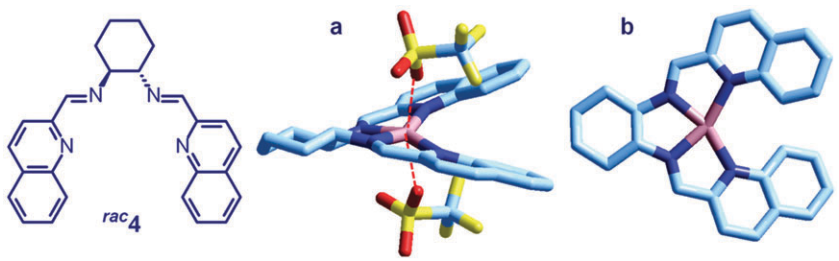

Fig. 14 Crystal and molecular structure of the complex salt $Cu^{II}(\mathbf{4})_2(CF_3SO_3)_2$;[22] the crystal contains the two enantiomeric forms: *P*-$Cu^{II}(^{SS}\mathbf{4})_2(CF_3SO_3)_2$ and *M*-$Cu^{II}(^{RR}\mathbf{4})_2(CF_3SO_3)_2$; the structure of the latter enantiomer is shown in the figure; (a) side view showing the axially bound triflate anions, in a very distorted elongated octahedral arrangement (Cu^{II}–O distance 2.43 Å, to be compared with the Cu–N distances: 1.96 Å, imine, and 2.01 Å quinoline); (b) top view without the triflate anions. Hydrogen atoms of the Schiff base ligand have been omitted for clarity.

from 0.13 to 0.36 Å. Moreover, the coordination sphere of the Cu^{II} cation also includes two oxygen atoms of the two triflate anions, which lie in the apical positions of a very elongated octahedron (Cu–O distances 2.43 Å, to be compared to the Cu–N distances 1.96 Å, imine, and 2.01 Å quinoline). The complex is indefinitely stable in an MeCN solution, where it is expected to maintain the same structural arrangement, with the poorly coordinating triflate anions replaced by solvent molecules.

On the other hand, ^{rac}**4** reacts with Cu^{I} salts to give dinuclear double stranded helicates, but the obtained crystalline complexes show distinct and surprising structural features, depending upon synthetic conditions.[22] Upon reaction of $[Cu^{I}(CH_3CN)_4]ClO_4$ with ^{rac}**4**, in a methanolic solution containing sodium triflate, the $[Cu^{I}_2(^{rac}\mathbf{4})_2](CF_3SO_3)_2{\cdot}H_2O$ complex salt was obtained. X-ray diffraction studies showed that each Cu^{I} ion is coordinated by two iminoquinoline subunits belonging to different molecules of **4**, with the two strands intertwined in a double helical arrangement. The crystal contains a 50/50 racemic mixture of the *homochiral* complexes *M*,*M*-$[Cu^{I}_2(^{RR}\mathbf{4})_2]^{2+}$ and *P*,*P*-$[Cu^{I}_2(^{SS}\mathbf{4})_2]^{2+}$, which confirms the principle of homochiral recognition in the formation of helicate complexes.[21] The structure of the *P*,*P*-$[Cu_2^{I}(^{SS}\mathbf{3})_2]^{2+}$ enantiomer is shown in Fig. 15a. Each Cu^{I} centre experiences a flattened tetrahedral geometry (Φ = 74°), with a metal–metal distance of 3.67 Å.

On the other hand, by reacting $[Cu^{I}(CH_3CN)_4]ClO_4$ with ^{rac}**4** in MeCN, dark purple crystals of $[Cu_2^{I}(^{rac}\mathbf{4})_2](ClO_4)_2{\cdot}H_2O$ were obtained. X-ray diffraction studies showed that the crystal contained two topological isomers: (i) the racemic mixture of the helicate complexes *M*,*M*-$[Cu_2^{I}(^{RR}\mathbf{4})_2]^{2+}$ and *P*,*P*-$[Cu_2^{I}(^{SS}\mathbf{4})_2]^{2+}$ (in Fig. 15b the latter enantiomer is shown) and (ii) a dinuclear complex in which the two strands were arranged side-by-side (Fig. 15c). In particular, the two strands of the side-by-side isomer are *heterochiral* and the complex is described by the formula *M*,*P*-$[Cu^{I}_2(^{RR}\mathbf{4})(^{SS}\mathbf{4})_2]^{2+}$. The racemic mixture and the side-by-side complexes were present in the crystal in a 2 : 1 ratio.

The helicate complex in Fig. 15b shows a rather constrained arrangement, with a short $Cu^{I}\cdots Cu^{I}$ distance (3.32 Å) and a heavily distorted tetrahedral coordination geometry (Φ = 68°), compared to the helicate complex shown in Fig. 15a ($Cu^{I}\cdots Cu^{I}$ distance 3.67 Å, Φ = 74°). The energy cost associated with these constraints is probably compensated by the establishment of a π–π interaction between two facing pyridine rings belonging to different strands (symbolised by a red dashed line in Fig. 15b). The two pyridine subunits are nearly parallel (angle between the two planes 11.9°) and the distance between their centroids is 3.45 Å. Notice that these geometrical features are common to the helicate complex *M*,*M*-$[Cu^{I}_2(^{RR}\mathbf{3})_2]^{2+}$, as shown in Fig. 13.

The side-by-side topological isomer shows distinct geometrical features with respect to the two helicate complexes. It shows a very long $Cu^{I}\cdots Cu^{I}$ distance (4.91) Å, while each metal centre experiences a nearly regular tetrahedral coordination geometry (Φ = 87.1°), which suggests an arrangement not affected by severe steric constraints. In any case, the energy difference between the three isomeric complexes isolated in the solid state should be rather small, as they coexist in the same crystal or their formation depends on poorly significant difference in the synthetic procedure.

As far as the solution behaviour is concerned, NMR spectra in CD_3CN solutions, prepared by dissolving the solid complex, either perchlorate or triflate, or by mixing equivalent amounts of **4** and $[Cu^{I}(CH_3CN)_4]ClO_4$, were identical and their features indicated that only two helical forms exist, one of which is more prevalent (87%, at 20 °C).[22] It can be hypothesised that the two forms correspond to the crystalline complexes of Fig. 15a and b (as a racemic mixture).

On the basis of structural and spectroscopic studies, it can be anticipated that the Cu^{II}/Cu^{I} redox change will give rise to helical assembling–disassembling processes in solution. Fig. 16 reports the CV profile taken at a platinum working electrode for an MeCN solution of $[Cu^{I}_2(^{rac}\mathbf{4})_2]^{2+}$, made 0.1 M in $[Bu_4N]ClO_4$.[22]

Upon oxidation of the $[Cu^{I}_2(^{rac}\mathbf{4})_2]^{2+}$ complex, which is present in solution in the helicate form, an anodic peak is observed at ~600 mV (zone I in the CV profile in Fig. 16). In the reverse reduction scan, a cathodic peak (zone II) develops at 50 mV. Such a behaviour can be interpreted on the basis of the square scheme shown in Fig. 12. The two-electron oxidation of $[Cu^{I}_2(^{rac}\mathbf{4})_2]^{2+}$ to give $[Cu^{II}_2(^{rac}\mathbf{4})_2]^{4+}$ is immediately followed by disassembling to two stable mononuclear complexes of $[Cu^{II}(^{rac}\mathbf{4})]^{2+}$. Their two-electron reduction to give the corresponding

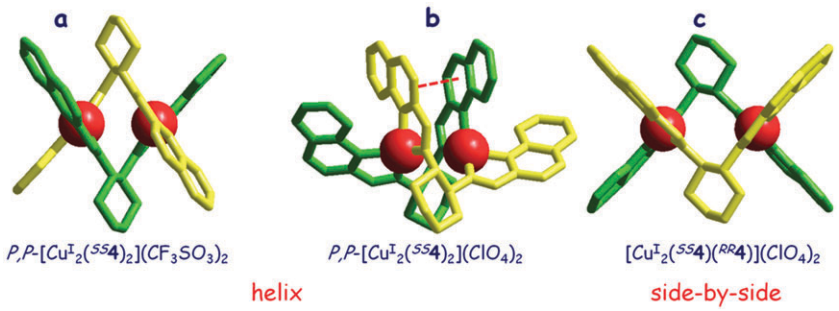

Fig. 15 (a) Structure of the *P*,*P*-$[Cu^{I}_2(^{SS}\mathbf{4})_2]^{2+}$ enantiomer, present in the racemic *triflate* complex salt (thus containing also the other enantiomer *M*,*M*-$[Cu^{I}_2(^{RR}\mathbf{4})_2]^{2+}$) which was obtained in an MeOH solution. Structures (b) and (c) refer to the dinuclear *perchlorate* complex salt obtained in MeCN.[22] The crystal contains (i) the racemic mixture of the homochiral helicate complexes *M*,*M*-$[Cu_2^{I}(^{RR}\mathbf{4})_2]^{2+}$ and *P*,*P*-$[Cu_2^{I}(^{SS}\mathbf{4})_2]^{2+}$ (the latter enantiomer reported in (b)) and (ii) the side-by-side dinuclear heterochiral complex (c). Counterions and ligand hydrogen atoms have been omitted for clarity.

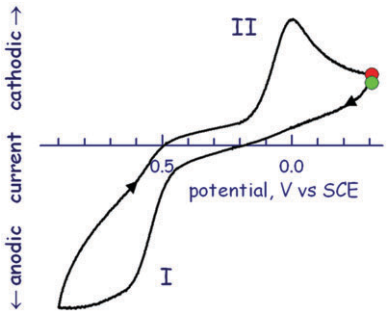

Fig. 16 CV profile obtained at a platinum working electrode for an MeCN solution of $[Cu^{I}_2(\mathbf{4})_2]^{2+}$, made 0.1 M in $[Bu_4N]ClO_4$. Potential scan rate: 100 mV s^{-1}. Starting point: −300 mV (green filled circle); end point: −300 mV (red filled circle). Scan was reversed at 800 mV *vs.* SCE. Diagram adapted from ref. 22.

$[Cu^{I}(^{rac}\mathbf{4})]^{+}$ complexes requires the achievement of a rather cathodic potential (zone II) and is followed by the immediate assembling to form the $[Cu^{I}_2(^{rac}\mathbf{4})_2]^{2+}$ helicate complexes. This behaviour is similar to that observed for the $[Cu^{I}_2(\mathbf{2})_2]^{2+}$ complex and is indicative of a poor stability of the dicopper(II) helicate complex.

5 Additional π–π interactions stabilise dinuclear helicates of copper(I) and copper(II)

It has been observed that π–π interactions of cofacial pyridine subunits belonging to different strands may contribute to stabilise the double helix arrangement in the two complexes *M*,*M*-$[Cu^{I}_2(^{RR}\mathbf{3})_2]^{2+}$ (Fig. 13) and *P*,*P*-$[Cu_2{}^{I}(^{SS}\mathbf{4})_2]^{2+}$ (that obtained as a perchlorate salt, whose structure is shown in Fig. 15b).

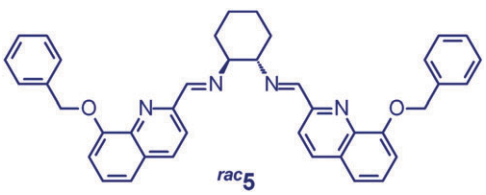

$^{rac}\mathbf{5}$

At this stage, we considered that more extended π–π interactions could provide further stabilisation of the double helix arrangement and favour the formation of both dicopper(I) and dicopper(II) helicates, thus imparting full reversibility to the voltammetric behaviour (if this can be considered a deserving achievement). For such a reason, we considered as a helicand the Schiff base $^{rac}\mathbf{5}$, which contains two more phenyl rings, appended to the two quinoline subunits through a $–CH_2O–$ bridge.[23]

Noticeably, the dicopper(I) complex displays the helical–non-helical dualism, which depends, again, on minimal differences in the isolation of the crystalline products. In fact, upon slow diffusion of diethylether in a solution containing equimolar amounts of $[Cu^{I}(MeCN)_4ClO_4$ and $^{rac}\mathbf{5}$, two different molecular and crystal structures were obtained, depending upon the solvent used, whether THF or MeCN.

In particular, (i) the blue crystal obtained from MeCN contained two solvate diethylether molecules, two perchlorate counterions, and the *heterochiral* dimeric molecular cations of formula *M*,*P*-$[Cu^{I}_2(^{RR}\mathbf{5})(^{SS}\mathbf{5})]^{2+}$, with a *side-by-side* arrangement of the two strands (Fig. 17a); (ii) the brown crystal obtained from THF contained a solvated water molecule, two perchlorate counterions and a racemic mixture of the two *homochiral* enantiomers $\{M,M\text{-}[Cu^{I}_2(^{RR}\mathbf{5})_2]^{2+} + P,P\text{-}[Cu^{I}_2(^{SS}\mathbf{5})_2]^{2+}\}$, both arranged in a *double-helical* fashion (Fig. 17b, the *P*,*P*-$[Cu^{I}_2(^{SS}\mathbf{5})_2]^{2+}$ enantiomer is shown). As observed in the case of dicopper(I) complexes of **4**, the side-by-side derivative seems to profit from a more relaxed conformational arrangement than the double helical analogue: in fact, the coordination geometry of each Cu^{I} centre is distinctly closer to a regular tetrahedron (Φ = 87.6° *vs.* 79.6°) and the $Cu^{I}\cdots Cu^{I}$ distance is appreciably higher (4.99 Å *vs.* 3.89 Å), which accounts for a lower electrostatic repulsion. On the other hand, two definite inter-ligand π–π interactions operate in the helical complex, involving a benzyloxy fragment of one strand (π-donor) and a metal coordinated pyridine ring of the other strand (π-acceptor). In particular, the distance between the centroids of the two rings is 3.63 Å (indicated as dashed red segments in Fig. 17b). In any case, these contrasting energy terms seem to balance in the

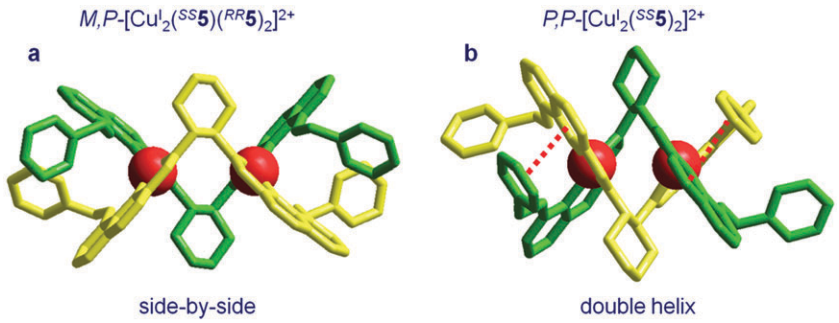

Fig. 17 Crystal structures of the dinuclear complexes obtained from the reaction of $[Cu^{I}(MeCN)_4ClO_4$ and $^{rac}\mathbf{5}$, in different solvents:[23] (a) in MeCN, blue crystals of *M*,*P*-$[Cu^{I}_2(^{RR}\mathbf{5})(^{SS}\mathbf{5})](ClO_4)_2\cdot(Et_2O)_2$, containing the *heterochiral* side-by-side derivative; (b) in THF, brown crystals of $[Cu^{I}_2(^{rac}\mathbf{5})_2](ClO_4)_2\cdot H_2O$, consisting of the racemic mixture of the two *homochiral* enantiomers $\{M,M\text{-}[Cu^{I}_2(^{RR}\mathbf{5})_2]^{2+} + P,P\text{-}[Cu^{I}_2(^{SS}\mathbf{5})_2]^{2+}\}$, in a *double-helical* arrangement. The *P*,*P*-$[Cu^{I}_2(^{SS}\mathbf{5})_2]^{2+}$ enantiomer is shown in the figure. Perchlorate counterions, solvate molecules and ligand hydrogen atoms have been omitted for clarity.

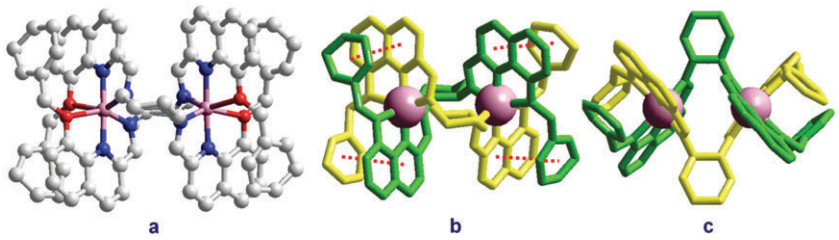

Fig. 18 Crystal and molecular structure of the *P,P*-$[Cu^{II}_2(^{RR}\mathbf{5})_2]^{4+}$ helicate complex, coexisting in the crystal with the *M,M*-$[Cu^{II}_2(^{SS}\mathbf{5})_2]^{4+}$ enantiomer (not shown);[23] (a) stick and ball model indicating that each Cu^{II} ion is six-coordinate, according to a distorted octahedral geometry. The donor set consists of two NNO terdentate subunit (imine nitrogen atom, quinoline nitrogen atom, benzyloxy oxygen atom) each from one of the two strands; (b) tube model in which the *four* inter-strand π–π interactions are symbolised with red dotted segments; (c) lateral view clearly showing the double helical arrangement.

solid state, considering that the two topological isomers coexist in the same crystal.

The big surprise came from the Cu^{II} behaviour. Upon slow diffusion of diethylether in a solution containing equimolar amounts of $Cu^{II}(CF_3SO_3)_2$ and $^{rac}\mathbf{5}$, red crystals of a compound of formula $[Cu^{II}_2(^{rac}\mathbf{5})_2]$ $(CF_3SO_3)_4$ were obtained. X-ray diffraction studies showed that crystals of the complex salt contained the racemic mixture of two enantiomeric homochiral double stranded helicate complexes. Fig. 18 shows three different views of the *P,P*-$[Cu^{II}_2(^{RR}\mathbf{5})_2]^{4+}$ cationic complex, present in the crystal with its enantiomer *M,M*-$[Cu^{II}_2(^{SS}\mathbf{5})_2]^{4+}$, at 50/50.

The ball and stick model (Fig. 18a) shows that each Cu^{II} centre is six-coordinate, according to a distorted octahedral geometry, through the binding of a NNO terdentate donor set (imine nitrogen atom, quinoline nitrogen atom, benzyloxy oxygen atom) from each strand. Bond distances are: Cu^{II}–$N_{quinoline}$: 1.95 Å, Cu^{II}–N_{imine} 2.11 Å, Cu^{II}–O 2.45 Å. Additional coordination by benzyloxy oxygen atoms may contribute to stabilise the Cu^{II} state, not necessarily the double helical arrangement. Such an arrangement is probably favoured by the establishment of *four* π–π interactions involving one benzyloxy ring and one pyridine ring of the quinoline subunit, belonging to two different stands (symbolised with red dashed lines in Fig. 18b). The distance between the centroids of the benzyl and pyridine rings is 3.62 Å, which indicates the existence of a π–π interaction similar to the one in the Cu^{I} helicate complex of **5** but occurring twice. Moreover, the coexistence in the crystal of enantiomers, each one constituted by two homochiral strands, demonstrates the general nature of the principle of chiral recognition in the formation of double stranded helicates, which was ascertained for spherical d^{10} metal ions (*e.g.* Cu^{I}),[21] and can be extended to the corresponding complexes of genuine transition metals (Cu^{II}, d^9). The establishment of four π–π interactions can account for the fact that we did not observe the formation of crystals containing the side-by-side topological isomer, in which benzyl and pyridine rings could not stack and interact each other. However, the dimeric Cu^{II} complex is not stable in an MeCN solution. In fact, the ESI mass spectrum of a solution containing equimolar amounts of $^{rac}\mathbf{5}$ and of $Cu^{II}(CF_3SO_3)_2$ showed a peak at 333.8 *m*/*z*, which corresponds to the monomeric complex $[Cu^{II}(\mathbf{5})]^{2+}$. In particular, the isotope pattern showed a peak-to-peak separation of 0.5 *m*/*z*, as expected for a monomeric species. It is possible that the energy term associated with coordination by the solvent is higher than the energy gain from inter-strand π–π interaction, thus favouring the formation of a mononuclear complex, whether five- or six-coordinate.

Fig. 19a illustrates the CV behaviour at the platinum working electrode of an MeCN solution containing equimolar amounts of $Cu^{II}(CF_3SO_3)_2$ and $^{rac}\mathbf{5}$. In the reduction scan (solid black line), a peak is observed at *ca.* 0 V *vs.* SCE, similar to the observed in the case of the $[Cu^{II}(^{rac}\mathbf{4})]^{2+}$ complex (see Fig. 16), which has to be ascribed to the one-electron reduction of the copper(II) monomeric complex to $[Cu^{I}(^{rac}\mathbf{5})]^{2+}$. Then, two $[Cu^{I}(^{rac}\mathbf{5})]^{2+}$ complexes self-assemble to give the dimeric $[Cu^{I}_2(^{rac}\mathbf{5})_2]^{2+}$ species. Upon the reverse oxidation scan, $[Cu^{I}_2(^{rac}\mathbf{5})_2]^{2+}$ undergoes two stepwise one-electron oxidation, to give dimeric copper(II) complexes. However, in the second reduction scan (dashed red line in Fig. 19a), no consecutive one-electron reduction peaks are observed, but the same reduction peak at *ca.* 0 V *vs.* SCE develops. This indicates that the dimeric $[Cu^{I}_2(^{rac}\mathbf{5})_2]^{2+}$ complex immediately disassembles to give two monomeric complexes again.

Fig. 19b shows the CV profile obtained at a platinum electrode for an MeCN solution 10^{-3} M both in $[Cu^{I}(MeCN)_4]ClO_4$ and in $^{rac}\mathbf{5}$, at a potential scan rate of 100 mV s^{-1}. Upon oxidation, two one-electron waves are observed, which are

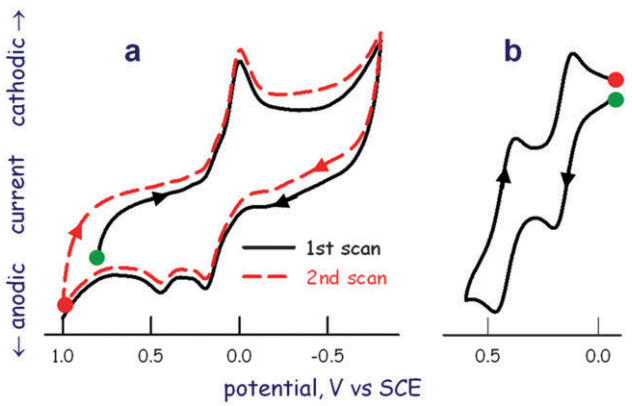

Fig. 19 CV profiles taken at the platinum electrode for an MeCN solution made 0.1 M in $[Bu_4N]ClO_4$ at 25 °C, with a potential scan rate of 100 mV s^{-1}: (a) 10^{-3} M both in $Cu^{II}(CF_3SO_3)_2$ and $^{rac}\mathbf{5}$; (b) 10^{-3} M both in $[Cu^{I}(MeCN)_4]ClO_4$ and in $^{rac}\mathbf{5}$. Diagrams adapted from ref. 23.

restored in the reverse scan, disclosing a fully reversible behaviour. This indicates that, before the scan begins, a dimeric $[Cu^{I}_2(^{rac}\mathbf{5})_2]^{2+}$ complex forms, which should be structurally different from that obtained upon reduction of $[Cu^{II}(^{rac}\mathbf{4})]^{2+}$ in the CV experiment described in Fig. 19a. The $[Cu^{I}_2(^{rac}\mathbf{5})_2]^{2+}$ complex of Fig. 19b is oxidised to a dimeric dicopper(II) complex. $[Cu^{I}_2(^{rac}\mathbf{5})_2]^{2+}$, which is stable in the time scale of the CV experiment at 100 mV s^{-1}. It is suggested that, in the experiment described by Fig. 19b, Cu^{I} and $^{rac}\mathbf{5}$ have all the time to arrange to a stable helicate structure, which is maintained after the stepwise oxidation. In contrast, the dicopper(I) species which forms after Cu^{II}/Cu^{I} reduction in the experiment in Fig. 15a probably cannot benefit from a time sufficiently long to rearrange to a stable double helix conformation and, when oxidised to Cu^{II}, immediately disassembles. One can speculate that side-by-side to double helical conversion and establishment of π–π interactions can play a role in the kinetically complicate rearrangement of the helicate to the more stable conformation.

$^{RR}\mathbf{6}$

At this stage, it was quite obvious to extend this type of study to the copper complexes of ligand **6**, which, for having a naphthyloxy substituent, is a candidate to establish more expanded inter-strand π–π interactions.[24] In this case, the *R*,*R* enantiomer was considered, which, upon reaction with an equimolar amount of $[Cu^{I}(MeCN)_4]ClO_4$, gave dark blue crystals of the $[Cu^{I}_2(^{RR}\mathbf{6})_2](ClO_4)_2{\cdot}4CH_3CN{\cdot}2H_2O$ complex salt. Fig. 20 shows the crystal and molecular structure of the homochiral double stranded helicate complex *M*,*M*-$[Cu^{I}_2(^{RR}\mathbf{6})_2]^{2+}$.

The most relevant structural feature is that all the four naphthalene rings are face-to-face stacked with respect to the four adjacent quinoline moieties, thus originating four inter-strand π–π interactions. The distance between the centroids of the facing pyridine ring and closest phenyl ring is 3.49 Å, to be compared with the value of 3.63 Å observed for the $[Cu^{I}_2(^{RR}\mathbf{5})_2]^{2+}$ analogue. As expected, the 2-naphtylmethoxy substituent favours the formation of extensive inter-strand π–π interactions. Just to make a well known example, the distance between two planes in graphite is 3.35 Å. The establishment of extended inter-strand π–π interactions occurs, apparently, without any serious conformational cost: for instance, the $Cu^{I}\cdots Cu^{I}$ distance is 3.84 Å to be compared with the value of 3.89 Å of the $[Cu^{I}_2(^{RR}\mathbf{5})_2]^{2+}$ complex. Unfortunately, no crystals were obtained from solutions of equimolar amounts of $Cu^{II}(CF_3SO_3)_2$ and $^{RR}\mathbf{6}$ in a variety of solvents. Also ESI mass spectroscopy investigations on an MeCN solution containing equimolar amounts of $^{RR}\mathbf{6}$ and $Cu^{II}(CF_3SO_3)_2$ did not give any definite information on the nuclearity of the copper(II) complex. In fact, the spectrum showed a peak at 768.7 *m*/*z*, corresponding to the species $[Cu^{I}_2(^{RR}\mathbf{6})_2]^{2+}$, while the isotope pattern showed a peak-to-peak separation of 0.5 *m*/*z*, thus indicating the presence of two copper ions. It has been observed that, under the drastic conditions of the ESI experiment, Cu^{II} complexes of ligands belonging to the family of **4**, **5** and **6** Schiff bases undergo spontaneous reduction to the corresponding dicopper(I) helicate,[25] but it is not possible to assess whether the reduction involves a dicopper(II) complex or a mononuclear Cu^{II} species, which, after reduction, assembles to give the helicate complex. However, more explicit information on the state of the copper(II) complex with $^{RR}\mathbf{6}$ came from CV studies.

Fig. 21a shows the CV profile obtained at the platinum electrode for an MeCN solution 10^{-3} M both in $Cu^{II}(CF_3SO_3)_2$ and $^{RR}\mathbf{6}$, made 0.1 M in $[Bu_4N]PF_6$ at 25 °C, at a potential scan rate of 100 mV s^{-1}. On the reduction scan, two consecutive peaks (I and II) are observed, which can be assigned to the two-step one-electron reduction of a dimeric copper(II) complex to give the dicopper(I) helicate complex (III and IV). The process is poorly reversible, in an electrochemical sense, as indicated by the quite large difference between corresponding reduction and oxidation peaks: $E_p(IV) - E_p(I) = 380$ mV; $E_p(III) - E_p(II) = 300$ mV (for a

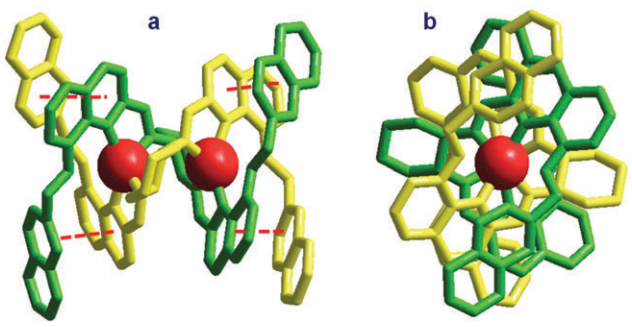

Fig. 20 Crystal and molecular structure of the $[Cu^{I}_2(^{RR}\mathbf{6})_2](ClO_4)_2{\cdot}4CH_3CN{\cdot}2H_2O$ complex salt (anions and solvate molecules have been omitted for clarity, as well as hydrogen atoms):[24] (a) lateral view of the *M*,*M*-$[Cu^{I}_2(^{RR}\mathbf{6})_2]^{2+}$ dication; (b) view along the axis containing the two Cu^{I} centres.

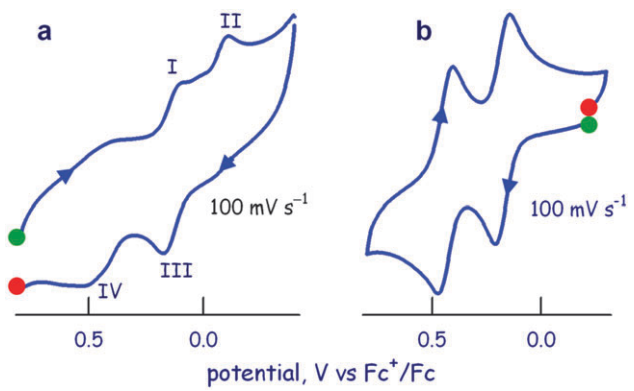

Fig. 21 CV profiles taken at the platinum electrode for an MeCN solution made 0.1 M in $[Bu_4N]PF_6$ at 25 °C, with a potential scan rate of 100 mV s^{-1}: (a) 10^{-3} M both in $Cu^{II}(CF_3SO_3)_2$ and $^{RR}\mathbf{6}$; (b) 10^{-3} M both in $[Cu^{I}(MeCN)_4]ClO_4$ and in $^{RR}\mathbf{6}$.[24]

fully reversible CV wave: ΔE_p = 59 mV). This may be indicative of a kinetically complicated rearrangement of the intertwined ligands, following the Cu^{II}/Cu^{I} redox change. On the other hand, the $[Cu^{I}_2(^{RR}\mathbf{6})_2]^{2+}$ complex disclosed on oxidation a fully reversible behaviour. In particular, Fig. 21b displays the CV profile obtained for an MeCN solution 10^{-3} M both in $[Cu^{I}(MeCN)_4]ClO_4$ and in $^{RR}\mathbf{6}$. The voltammogram shows on the oxidation scan two well defined waves, fully reversible in the reverse reduction scan, with a peak separation of 59 mV for each wave.

It should be noted that the separation of the two half-wave potentials, $\Delta E_{1/2}$ = 262 mV, is associated with the comproportionation equilibrium:

$$[Cu^{II}_2(^{RR}\mathbf{6})_2]^{4+} + [Cu^{I}_2(^{RR}\mathbf{6})_2]^{2+} \leftrightarrows 2[Cu^{II}Cu^{I}(^{RR}\mathbf{6})_2]^{3+} \qquad (2)$$

The higher ΔE, the more favored the comproportionation equilibrium (2). In particular, the comproportionation constant K_C is related to ΔE through the following equation:[26]

$$K_C = e^{\frac{\Delta E \times F}{R \times T}} \quad \left\{ \text{at 298 K} : K_C = e^{\frac{\Delta E}{25.69}} \text{ when } \Delta E \text{ is expressed in mV} \right\} \qquad (3)$$

Three main terms may contribute to ΔE, thus to the magnitude of the comproportionation constant K_C: (i) a statistical contribution of 35.61 mV; (ii) an electrostatic term, which results from the Coulombic repulsions between the metal ions in the two sides of the comproportionation equilibrium (2). In particular, in the left side, the following repulsions operate: $(1 \times 1) + (2 \times 2) = 5$ positive charges, whereas in the right side the number positive charges amounts to $2 \times (1 \times 2) = 4$, a circumstance which favours the displacement of equilibrium (1) to the right; (iii) a magnetic interaction between two metal centers in a given oxidation state: this could be the case of Cu^{II} (d^9) ions, which possess one unpaired electron and are therefore inclined to spin pairing, but the large distance between metal centers and the absence of any bridging ligand preclude any magnetic interaction. Thus, the magnitude of ΔE should be essentially controlled by the repulsive electrostatic term. It should be noticed that the value $\Delta E_{1/2}$ associated with the formation of the $[Cu^{II}Cu^{I}(^{RR}\mathbf{6})_2]^{3+}$ mixed valence complex ($\Delta E_{1/2}$ = 262 mV) is rather close to that observed for the corresponding $[Cu^{II}Cu^{I}(^{rac}\mathbf{5})_2]^{3+}$ analogue ($\Delta E_{1/2}$ = 280 mV). This seems reasonable, as the $Cu^{I}\cdots Cu^{I}$ distances for $^{RR}\mathbf{6}$ and $^{RR}\mathbf{5}$ helicate complexes are quite similar: 3.84 Å and 3.89 Å, respectively, from which electrostatic repulsive effect of similar intensity should derive. On the other hand, the $\Delta E_{1/2}$ value associated with the formation of the $[Cu^{II}Cu^{I}(\mathbf{1})_2]^{2+}$ quaterpyridine complex is distinctly lower (190 mV), and the mixed valence complex less stable, in spite of the fact that the $Cu^{I}\cdots Cu^{I}$ distance (3.90 Å) is nearly the same as observed for the $[Cu^{I}_2(^{RR}\mathbf{5})_2]^{2+}$ and $[Cu^{I}_2(^{RR}\mathbf{6})_2]^{2+}$ complexes. In the absence of structural data on mixed valence complexes, any intepretation is very tentative. At this stage, however, one could suggest that the entirely π-conjugate system **1** is able to shield metal–metal Coulombic repulsions more effectively than Schiff base derivatives **5** and **6**.

6 Conclusion

Assembling molecular strands in a double helix mode results from the establishment of fast and reversible non-covalent interactions, a phenomenon which pertains to the realm of supramolecular chemistry. In nucleic acids, each one of the two strands brings its binding sites (nucleobases) and the formation of the double helix does not need any templating agent. In contrast, polynuclear helicates need a template (the metal ions), on which the two strands enfold themselves. Removal of the template (demetallation) makes the strands separate and diffuse in the solution. In the case of dinuclear helicates, disassembling can be induced by changing the properties of templating metals through a redox change: from an oxidation state prone to tetrahedral coordination (*e.g.* Cu^{I}), compatible with a dimeric double-strand arrangement, to an oxidation state strongly inclined toward tetragonal coordination (*e.g.* Cu^{II}), which can be better achieved through the formation of a mononuclear complex. However, disassembling can be made more difficult or prevented by equipping strands with additional binding sites (*e.g.* π-donor/acceptor substituents), which provide further stability to the double helix. It should be noted that such an additional energy contribution is present also in nucleic acids, associated with π–π interaction between stacked base pairs.

Helicands obtained through Schiff base condensation display a further intriguing property, related to the 'reversibility' of the C═N imine bond (*i.e.* to its ability to react with water to give original amine and aldehyde, according to a fast equilibrium).[27] It has been demonstrated that addition of a templating metal centre (*e.g.* Cu^{I}) to a mixture of dialdehydes, amines and aminoquinolines, which contained all possible imine condensation product in equilibrium, eliminated all partially formed and mixed imine ligands from the mixture and left the helicates as exclusive products.[28] We believe that, if the lability of the Cu–N coordinative interaction and the reversibility of the C═N bond are combined with the fast and reversible Cu^{I}/Cu^{II} redox change, new selective processes of assembling–disassembling supramolecular structures, including helicates, can be promoted.

Acknowledgements

The financial support of the Ministry of University and Research (PRIN: InfoChem) is acknowledged.

References

1 S. N. Kramer, *Sumerian Mythology*, University of Pennsylvania Press, Philadelphia, 1961.
2 E. Hamilton, *Mythology: Timeless Tales of Gods and Heroes*, Little, Brown and Company, New York, 1942.

3 http://www.sanmichelepavia.it/.
4 J. D. Watson and F. H. C. Crick, *Nature*, 1953, **171**, 737–738.
5 C. M. Henry, *Chem. Eng. News*, 2003, **81**, 49–60.
6 J.-M. Lehn, A. Rigault, J. Siegel, J. Harrowfield, B. Chevrier and D. Moras, *Proc. Natl. Acad. Sci. U. S. A.*, 1987, **84**, 2565–2569.
7 B. Dietrich, J. M. Lehn and J. P. Sauvage, *Tetrahedron Lett.*, 1969, 2889–2892.
8 M. Albrecht, *Chem. Rev.*, 2001, **101**, 3457–3497.
9 T. M. Garrett, U. Koert, J.-M. Lehn, A. Rigault, D. Meyer and J. Fischer, *J. Chem. Soc., Chem. Commun.*, 1990, 557–558; M. Barley, E. C. Constable, S. A. Corr, R. C. S. McQueen, J. C. Nutkins, M. D. Ward and M. G. B. Drew, *J. Chem. Soc., Dalton Trans.*, 1988, 2655–2662; C. Piguet, G. Bernardinelli and A. F. Williams, *Inorg. Chem.*, 1989, **28**, 2920–2925.
10 C. Piguet, G. Bernardinelli, B. Bocquet, A. Quattropani and A. F. Williams, *J. Am. Chem. Soc.*, 1992, **114**, 7440–7451; R. Krämer, J.-M. Lehn, A. DeCian and J. Fischer, *Angew. Chem., Int. Ed.*, 1993, **32**, 703–706.
11 R. G. Pearson, *J. Chem. Educ.*, 1968, **45**, 581–587; R. G. Pearson, *J. Chem. Educ.*, 1968, **45**, 643–648.
12 P. Tomislav, *Acta Crystallogr., Sect. E: Struct. Rep. Online*, 2006, **62**, m620–m622.
13 H. Nakai, *Bull. Chem. Soc. Jpn.*, 1983, **56**, 1637–1641.
14 M.-M. Yu, Y.-N. Zhang and L.-H. Wei, *Acta Crystallogr., Sect. E: Struct. Rep. Online*, 2007, **63**, m2380.
15 A. Livoreil, C. O. Dietrich-Buchecker and J.-P. Sauvage, *J. Am. Chem. Soc.*, 1994, **116**, 9399–9400; for a recent reviews on movable catenates see: S. Durot, F. Reviriego and J.-P. Sauvage, 2010, **39**, 10557–10570.
16 V. Amendola, L. Fabbrizzi, C. Mangano and P. Pallavicini, *Acc. Chem. Res.*, 2001, **34**, 488–493.
17 A.-M. Stadler, C. Burg, J. Ramirezd and J.-M. Lehn, *Chem. Commun.*, 2013, **49**, 5733–5735.
18 J.-P. Gisselbrecht, M. Gross, J.-M. Lehn, J.-P. Sauvage, R. Ziessel, C. Piccinni-Leopardi, J. M. Arrieta, G. Germain and M. Van Meerssche, *Nouv. J. Chim.*, 1984, **8**, 661–667.
19 J.-M. Lehn, J.-P. Sauvage, J. Simon, R. Ziessel, C. Piccini-Leopardi, G. Germain, J.-P. Declercq and M. Van Meersche, *Nouv. J. Chim.*, 1983, **7**, 413–420.
20 K. T. Potts, M. Keshavarz-K, F. S. Tham, H. D. Abruna and C. R. Arana, *Inorg. Chem.*, 1993, **32**, 4422–4435.
21 M. A. Masood, E. J. Enemark and T. D. P. Stack, *Angew. Chem., Int. Ed.*, 1998, **37**, 928–932.
22 V. Amendola, L. Fabbrizzi, L. Linati, C. Mangano, P. Pallavicini, V. Pedrazzini and M. Zema, *Chem.–Eur. J.*, 1999, **5**, 3679–3688.
23 V. Amendola, M. Boiocchi, V. Brega, L. Fabbrizzi and L. Mosca, *Inorg. Chem.*, 2010, **49**, 997–1007.
24 M. Boiocchi, V. Brega, C. Ciarrocchi, L. Fabbrizzi and P. Pallavicini, *Inorg. Chem.*, 2013, **52**, 10643–10652.
25 L. Gianelli, V. Amendola, L. Fabbrizzi, P. Pallavicini and G. G. Mellerio, *Rapid Commun. Mass Spectrom.*, 2001, **15**, 2347–2353.
26 D. E. Richardson and H. Taube, *Inorg. Chem.*, 1981, **20**, 1278–1285.
27 M. E. Belowich and J. F. Stoddart, *Chem. Soc. Rev.*, 2012, **41**, 2003–2024.
28 M. Hutin, R. Frantz and J. R. Nitschke, *Chem.–Eur. J.*, 2006, **12**, 4077–4082.